WILEY | Hindawi

Research Article

Posture Risk Assessment and Workload Estimation for Material Handling by Computer Vision

Ziao Wang [iD],[1] **Weixing Wang** [iD],[1,2] **Jingxi Chen** [iD],[1] **Xuzhuang Zhang** [iD],[1] **and Ziheng Miao** [iD][2]

[1]*School of Mechanical Engineering, Guizhou University, Guiyang, China*
[2]*Key Laboratory of Advanced Manufacturing Technology, Ministry of Education, Guiyang, China*

Correspondence should be addressed to Weixing Wang; wxwang1@gzu.edu.cn

Workers in material handling tasks often suffer from work-related musculoskeletal disorders (WMSDs) caused by inaccurate work postures or the lifting of excessively heavy loads. Therefore, effective ergonomic assessment of workers is needed to improve worker productivity while reducing the risk of musculoskeletal disorders. This paper proposes a noninvasive method for evaluating posture risks and load analysis in manual material handling tasks. The study focuses on three main aspects: first, using 3D pose recognition technology to extract the 3D coordinates and joint angles of the human body. Second, the REBA method was improved by using fuzzy logic theory to more effectively capture the slow transition features of continuous movement by humans without abruptly altering risk scores, as well as to increase the accuracy and consistency of posture risk evaluation. Third, joint torque and workloads were estimated using biomechanical calculations by integrating pressure insoles and 3D joint coordinate data. Experiments show that this method can effectively evaluate posture risks and workloads in manual material handling tasks, with a correlation coefficient of 0.817 ($p < 0.01$) between fuzzy logic REBA and REBA and an error rate of 15% in estimating workloads of eight joints. This method can help reduce occupational health risks for workers and industries and improve work efficiency.

1. Introduction

Manual material handling (MMH) operations are commonly found in many industries such as manufacturing, logistics, and construction. Due to the repetitive and awkward nature of these tasks, workers often experience discomfort and overexertion issues [1, 2], which can lead to work-related musculoskeletal disorders (WMSDs). Especially in developing countries, many industries cannot meet the demand for automation, and most productive work is still done through semiautomatic means. Since WMSDs have early symptoms that are not always obvious, the onset of the disease is often delayed. Workers frequently ignore them. Continuous improper working posture not only endangers workers' health but also results in decreased productivity, reduced production capacity [3], and economic losses. Therefore, effective risk assessment and load analysis methods must be developed for MMH operations to prevent WMSDs and improve worker health and safety.

Effective human-machine ergonomic evaluation to avoid ergonomic risks in the work process is currently the mainstream research direction for reducing the incidence of WMSDs.

Manual observation methods and wearable inertial sensors are widely used in ergonomic postural risk assessment, and although these studies have demonstrated the feasibility of the methods, they still have some limitations [4, 5]. The results of manual observation are subjective, and different observers may give different assessments based on the same posture. Wearable sensors can capture body joint information more objectively and accurately, but this approach requires multiple sensors on the operator, which can interfere with normal work and is invasive.

Therefore, more practical and effective methods are needed to assess posture and load risks in MMH operations [6]. With the development of computer vision technology, it

is now possible to recognize human posture by using human pose estimation technology to capture images or video frames of people at work. After obtaining the worker's pose skeletal data, WMSD risk assessment can be conducted using risk assessment rules. This approach is currently a trend in machine vision-based human-machine engineering risk assessment [7]. However, there are still some issues to be addressed. Most of the current research is directly applying the rules of the traditional postural risk assessment method to the vision-based risk assessment system. The joint angles recognized and calculated by posture are more accurate, while the range of motion of the joint angles of the traditional risk assessment method goes to give a generalized score, so there are some problems in combining the traditional assessment method with the vision-based risk assessment. How to improve the traditional assessment method to be able to more accurately conduct operational risk assessment and make it more suitable for vision-based risk assessment is the current research gap. Also, the vision-based risk assessment is only applicable to activities with a large amplitude of joint movement; for some activities with a more fixed posture but at the same time cause a large load on the body (material handling, etc.), only the elbow joint has a large amplitude of movement, so the overall risk score will be low, but the activity of the human impact is large. Therefore, it is possible to analyze the joint loads by combining the known joint point information from the posture estimation with the external loads, i.e., to assess the operational risk from another perspective. Therefore, combining human postural risk and joint load assessment is meaningful and can improve the whole ergonomic posture risk assessment more.

In this study, we propose a novel method that combines human pose recognition, pose risk assessment, and biomechanical load analysis to evaluate the posture risk and joint loads during manual material handling (MMH) operations. The present method enables accurate and noninvasive monitoring and evaluation of workers' body posture while taking into consideration the dynamic aspects of loads, risks, and posture during the job process. The following are the study's primary contributions:

(1) The proposed approach can accurately identify the workers' full-body posture, improving the visual recognition performance under occlusion conditions

(2) The traditional REBA risk assessment method is improved to avoid the problem of sudden changes in REBA assessment scores due to changes in joint angle inputs, making it more suitable for machine vision-based job risk assessment

(3) A method combining computer vision technology and sensors is proposed to monitor the joint torques and workloads through a new noninvasive means

The remainder of this paper is organized as follows: In Section 2, we present related work on ergonomic posture risk assessment as well as biomechanically-based human load assessment and further summarize the gaps in the current research area. Section 3 presents models for human

posture estimation, transformations for joint angle calculation, fuzzy logic-based REBA risk assessment, and finally, biomechanically-based load estimation. Section 4 describes the whole experimental environment as well as the experimental flow and experiments on the comparison of joint recognition accuracy by IMU sensors with the proposed method. In Section 5, we further carry out experiments on the comparison of REBA with the improved REBA and experimental results on the joint torque and joint loading evaluation, as well as discuss the superiority of the proposed method, and finally, Section 6 summarizes the work of the paper.

2. Related Work

2.1. Current Status of Ergonomic Posture Risk Assessment. Ergonomic postural risk assessments (EPRA) are commonly used to identify potential risks of WMSDs such as poor posture and repetitive movements [8]. These methods rely on on-site observation or video examination of joint angles between body parts, such as OWAS [9], NOISH [10], REBA [11], and RULA [12]. The Rapid Entire Body Assessment (REBA) is a typical assessment method that reduces the risk of WMSDs by evaluating the degree of loading of postures and movements on the body of the workers and then taking preventive measures according to the different risk levels. The REBA assessment process is divided into four parts: observation: observe the postures and movements of the workers, with special attention to the position of their limbs and the amplitude of their movements; scoring: use the REBA scale to assign corresponding scores to each body part and movement according to different body parts and movements, assigning a corresponding score to each body part and movement; analysis: calculating the overall score based on the scores and determining the risk level of the postures and movements based on the scoring results; and recommendations: suggesting corresponding improvements based on the assessment results to reduce the physical loads on the workers and reduce the risk of injury. However, manually completed EPRA may lead to several problems. First, EPRA results may be affected by the researcher's perspective and fatigue. Second, manual observation and assessment are more subjective and time-consuming.

Therefore, current research has seen the emergence of new techniques to replace manual assessment. These techniques fall into two categories: contact sensor methods and methods for noncontact vision. Different methods of risk assessment of body postures, both invasive and noninvasive, are shown in Table 1. The contact sensor approach consists of attaching sensors to the subject to collect musculoskeletal and motor data during work [13, 19]. Common sensors include motion capture systems and inertial sensors. This approach allows for an objective assessment of WMSDS risk [20]. However, as an invasive method, workers may be hindered from wearing sensors while working, and the high cost of various testing instruments and the time-consuming testing process can only be analyzed and tested in the laboratory, which makes it difficult to be widely applied in actual production activities. Therefore, the noncontact

TABLE 1: Different methods of human posture risk assessment.

Category	Device	Approach	Contribution	References
Contact sensor method	MoCap	Collect joint coordinates	An inertial sensor approach was developed to evaluate the working posture of workers on an automotive assembly line	[13]
	IMU sensor	Collect joint coordinates	A real-time motion alert personal protective equipment (PPE) based on a wearable inertial measurement unit (Wimu) was developed to enable workers to self-awareness and self-management of ergonomic hazardous operating modes to prevent WMSDs	[14]
	Kinect v2	Human key point recognition	Proposing a semiautomatic RULA evaluation software based on Microsoft Kinect v2 depth camera	[15]
	Kinect v2	Depth image acquisition and segmentation	A skeleton less holistic pose analysis system is proposed to accurately predict operational pose limb angles from a single depth image	[16]
Noncontact vision method	RGB-D camera	2D pose estimation based on CEPARA	A PAS-oriented holistic pose acquisition and ergonomic risk analysis model is proposed for developing a smartphone-based and workplace-based WMSDs risk assessment system	[17]
	RGB-D camera	2D pose estimation	A proposed vision-based real-time RULA method for scoring RULA levels of individual images captured by ordinary RGB cameras	[18]
	RGB-D camera	3D pose estimation based on 3DMPPE	The body angle reliability decision making (BARD) method is proposed to calculate the most reliable body bending angle	[2]

vision method has a wider application value. Using a single RGB camera for image recognition in human-machine risk assessment has become a current research trend [21–23]. Li et al. [18] proposed a real-time estimation method of RULA based on a deep neural network for two-dimensional joint pose, which first uses 2D action recognition to identify the skeleton points of the human body before using a 3D neural network to identify the positions and vectors of each joint. Next, by projecting the human body joints onto a sagittal plane in a similar way to projection, the angles between the joints are calculated to perform the RULA evaluation. Lee and Lee [17] proposed a human-machine engineering risk assessment system SEE, which combines the convolutional pose machine (CPM) method with a fast full-body assessment method. It can capture the overall human body posture for ergonomic risk analysis and only requires the input of posture video frames or images captured by a single camera. The system can also be used to develop WMSD risk assessments based on smartphones. Wang et al. [24] proposed an approach for predicting work-related musculoskeletal disorders (WMSD) that integrates three artificial intelligence algorithms and utilizes dynamic characteristics of working posture. A posture risk assessor examines the working posture's danger level frame by frame, while a posture detector detects the angles and states of the limbs. A task risk predictor is also used to forecast the risk level of the present work process.

2.2. Current Status of Biomechanically Based Human Load Assessment.

Biomechanical analysis is a method of measuring the load on the human body by evaluating joint forces or torques. It simplifies human joint activity as a hinge linkage mechanism. The joint torque is estimated by mechanical calculations and based on the human joint position, anthropometric characteristics, and external loads [25]. Workload evaluation has been performed in a variety of contexts using biomechanical analysis, including physical and cognitive workloads [26, 27]. Theoretically, biomechanics encompasses all critical components of workload evaluation, including intensity, repetitiveness, external load duration, and posture. Almost any action or body component may be studied using biomechanical analysis, including reiterated motion and static external load [28]. However, there is a gap between theoretical analysis and actual application, mostly because motion and external load data collection techniques are inexact. Although observation has been employed extensively to gather motion data, its results are thought to be too arbitrary and unreliable to support biomechanical research [29, 30]. Therefore, we need more accurate and automated data collection methods. Kim et al. [31] proposed a method to estimate human joint torque changes in real time while performing a large number of manipulation tasks by collecting joint position information and ground reaction force through experimenters wearing motion capture suits and standing on a force plate. However, wearable motion capture suits will affect people's normal work, as well as the limited movement of people standing on the force plate may not be suitable for practical applications.

In addition, human-machine simulation software such as OpenSim and anyone can perform muscle-driven dynamic simulations, providing a viable approach to analyzing the force and torque of elements in the musculoskeletal system and assisting in the evaluation of human load [32–34]. Human load assessment using computer vision is also a trend in research, as exemplified by the theoretical method proposed by Yang et al. [35] to analyze video tracking postures using a biomechanical model. By representing the biomechanical skeleton of the human body and evaluating workload and joint torque quickly and accurately based on joint rotation angle, the method can be used for work-related tasks. Kong et al. [36] proposed a 3D biomechanical model based on computer vision technology to study workers' mechanical energy consumption by approximating the working posture coordinates of human joints with a 2D video-based human body 3D pose estimation algorithm and using smart insoles to collect foot pressure and acceleration as input data for biomechanical analysis. The total maximum daily consumption of building tasks can be approximated through tasks such as walking, lifting, and bending. Currently, a new type of foot pressure sensor called Moticon is applied in biomechanical load analysis. The sensor can be used with almost any shoe, and smart insoles on the market can transmit data through wireless ANT services. Afari et al. [37] demonstrated the use of smart insoles to obtain the foot pressure of construction workers.

To summarize, most of the current machine vision-based operational pose risk assessment approaches directly apply the assessment logic of traditional analytical assessment approaches (e.g., RULA and REBA) directly to pose risk assessment. However, there is a serious problem with this approach, i.e., the sensitivity of the traditional assessment methods to the input variables is very low. For example, with REBA, 45° and 90° of flexion do not affect the upper arm score. On the contrary, a risk score of 2 when the torso is flexed 20° and 3 when the torso is flexed 21° may result in two different final values of REBA, which may affect the risk scoring level, as highlighted by previous studies [38, 39]. Thus, there are some problems in directly integrating the traditional observational assessment method into machine vision-based risk assessment. There is a need to improve the operational posture of wind assessment hair to make it more suitable for risk assessment via machine vision. Our approach is to perform operational risk assessment in a non-invasive way and to improve the traditional REBA approach by introducing the fuzzy logic method, so that the results of the assessment will not increase or decrease abruptly after the input of joints. The method is able to reflect the gradual transition characteristics of critical angles during human movement without sudden changes in risk ratings. Currently, in the biomechanical load assessment research, most of the studies are conducted through wearable motion capture suits, force plates, and other invasive devices to collect and calculate biomechanical loads, which will restrict the normal mode and range of human activities and are difficult to be applied to actual production, as well as some biomechanical assessment through human-computer simulation software that does not have real-time performance.

Therefore, we obtain the human reaction force by means of the pressure insole, and calculate the joint torques and joint workloads by combining the human joint position information and joint angles collected in the risk assessment part, and combine the two parts of the assessment with each other to make the overall ergonomics assessment more complete.

3. Methods

This research proposes a machine vision-based postural risk assessment methodology designed to capture the ability to monitor, assess, and predict the level of risk of work-related cumulative musculoskeletal disorders (WMSDs) from job videos and from pressure sensor data. The general architecture of the proposed method is shown in Figure 1:

(1) A monocular camera is used to capture video frames of a worker during operation, and then 2D human pose estimation is utilized to obtain 2D joint point information of the human body. The 3D pose estimation method is then utilized to predict the position of each joint point of the worker in 3D space and finally calculate the limb angle.

(2) The joint angles are input into the FREBA model for risk assessment. The model uses a fuzzy logic approach, which includes the steps of constructing the affiliation function, fuzzification, fuzzy reasoner, and defuzzification.

(3) Pressure sensors are placed inside the shoes of the operator to obtain the pressure data of the bottom of the foot during the operation, and the external load data are obtained by subtracting their own gravity. At the same time, the three-dimensional information of each joint point of the operator at this time is combined with the joint torques of the body parts, and, finally, the joint workload is calculated according to the load-bearing capacity of the joints.

3.1. Human Pose Estimation Model.

We collected workers' job video frames and used an open-source toolkit called MMpose to obtain their pose information. MMpose is an open-source framework based on PyTorch, which provides a set of reusable models, datasets, and tools for training and evaluating human pose estimation models. The framework utilizes state-of-the-art deep learning algorithms and has been extensively tested on multiple datasets, demonstrating good performance in the field of human pose estimation.

We used a top-down pose estimation recognition method and processed the collected video frame sequences using three different neural network models, as shown in Figure 2. The pose recognition model is divided into three modules. First, we used the faster-RCNN network [40] as the object detection layer to capture the worker's position information. Next, we used the HRNet [41] network model to recognize the 2D human body pose keypoint data of the worker and extract 16 key points. Finally, we used Video-Pose3D to convert the 2D keypoint prediction results into 3D coordinates, predicting the position information of each keypoint of the worker in the 3D coordinate system. VideoPose3D [42] employs the Hourglass network, which enables simultaneous consideration of both the local area and the entire image features. This network establishes a link between pixels or sets of pixels and multilayer neural networks, resulting in a comprehensive description. The entire pose recognition model was trained on the COCO dataset, aiming to transform the input video into human body key points and expand to the relative 3D position of each joint.

After identifying the 3D pose of the human body, we can extract the corresponding 3D positional data of each joint. However, in order to evaluate the posture using REBA, we also need to calculate the joint vectors and their specific angles using trigonometric functions. The joint coordinates are defined as $p_i = (x_i, y_i, z_i)$ and $p_{i+1} = (x_{i+1}, y_{i+1}, z_{i+1})$, and the limb is constructed by the adjacent key points p_i and p_{i+1}. The limb l_i is composed of the adjacent key points p_i and p_{i+1}, with $l_{ii+1} = \overline{p_i p_{i+1}}$ representing the limb. The absolute angle θ_i of limb l_i is determined by the expression $|y_{i+1} - y_i|$:

$$\theta_i = \tan^{-1} \frac{|y_{i+1} - y_i|}{\sqrt{(x_{i+1} - x_i)^2 + (z_{i+1} - z_i)^2}}. \tag{1}$$

During posture estimation, certain limb angles may be influenced by other body parts (e.g., the exact angle of the forearm may be impacted by the upper arm's position). As a result, the relative posture angle of the forearm concerning the upper arm must be calculated. The formula used to calculate the relative angle θ_i' between limb l_i and limb l_{i-1} is given by

$$\theta_i' = \cos^{-1} \frac{\overline{p_i p_{i+1}} \cdot \overline{p_{i-1} p_i}}{|\overline{p_i p_{i+1}}||\overline{p_{i-1} p_i}|}. \tag{2}$$

By calculating and converting the joint angles we, as shown in Figure 3, can see the positions of the different joint angles represented in the human skeletal points, which were calibrated at 11 joint angles in order to be used in the REBA postural risk assessment.

3.2. Fuzzy Logic REBA Risk Assessment.

The proposed fuzzy logic REBA assessment is based on the REBA method proposed by Hignett and Mcatamney [11]. REBA is an observational method to estimate whether work poses a potential health hazard by scoring the postural action ergonomics assessment method. However, the traditional REBA cannot be directly integrated into the risk assessment of machine vision. While the joint angles estimated by posture recognition techniques are very precise, even a small adjustment of 1° or even 0.001° in the joint angle can lead to sudden changes in the integer risk rating when input into REBA.

The input joint angle section necessitates the creation of affiliation functions for all model variables. These fuzzy membership functions enable the mapping of a collection of objects X in the range [0, 1], allowing for numerical calculations in afterward fuzzy inference processes. In the
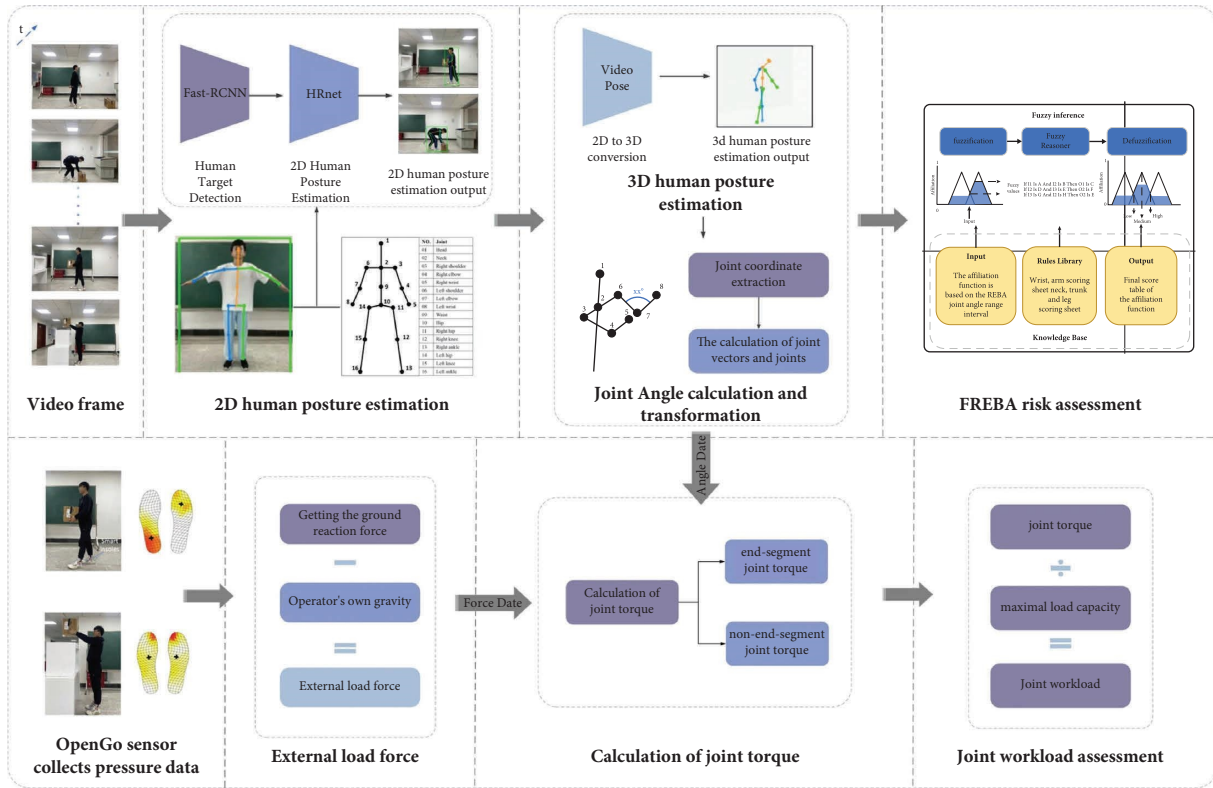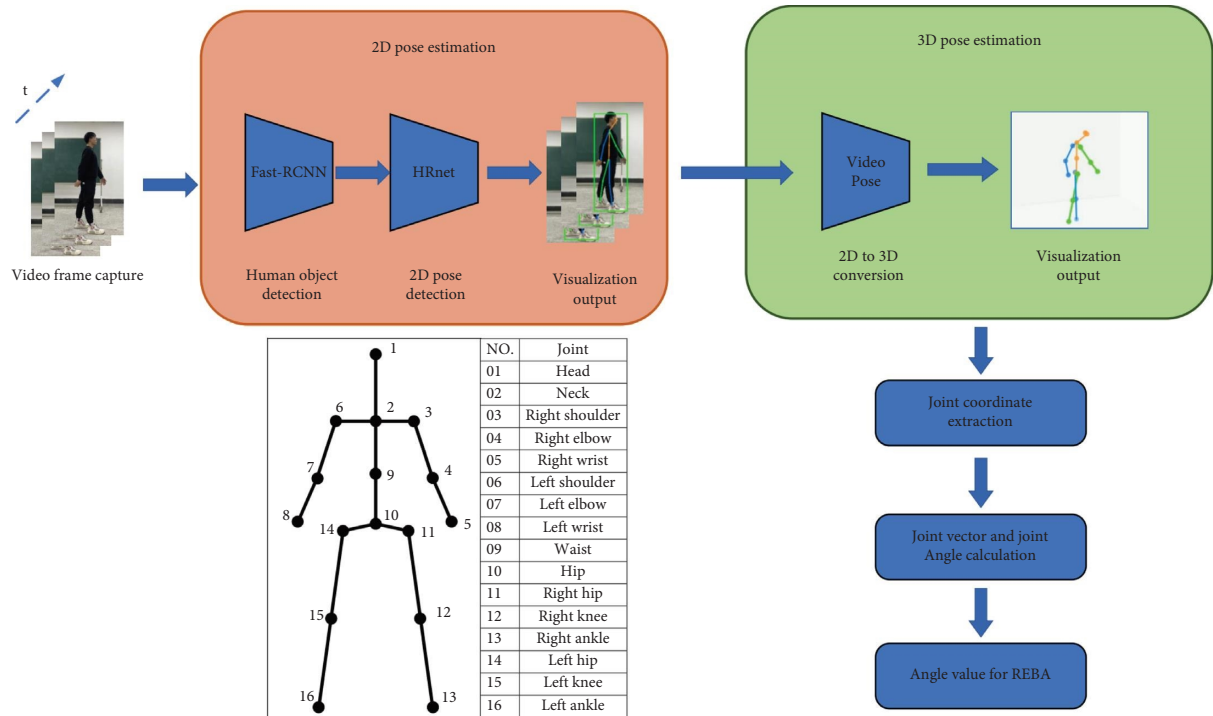
Figure 1: Overall research process.

Figure 2: Human body posture estimation process and human skeletal diagram.
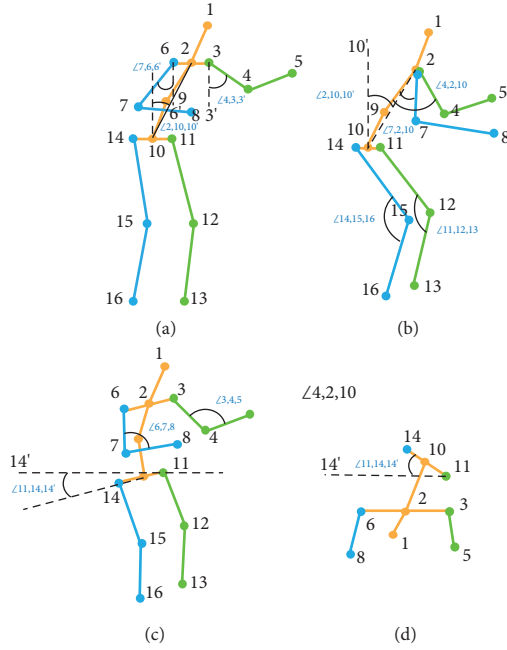
FIGURE 3: Schematic representation of joint angle and location.

Table: Corresponding 11 joint angles

Joint Angle Name	Angle Location
Left Shoulder Lift Angle	∠4,2,10 in Fig. 3b
Right Shoulder Lift Angle	∠7,2,10 in Fig. 3b
Left shoulder abduction angle	∠4,3,3' in Fig. 3a
Right shoulder abduction angle	∠7,6,6' in Fig. 3a
Left elbow position angle	∠3,4,5 in Fig. 3c
Right elbow position angle	∠6,7,8 in Fig. 3c
Left knee flexion angle	∠11,12,13 in Fig. 3b
Right knee flexion angle	∠14,15,16 in Fig. 3b
Trunk flexion angle	∠2,10,10' in Fig. 3a
Trunk bending angle	∠2,10,10' in Fig. 3b
Trunk twisting angle	∠11,14,14' in Fig. 3d

context of the REBA method, the body is divided into two main sections. The neck, trunk, and legs make up the first part, and Table A [11] in the REBA worksheet aggregates their respective scores. The second part of REBA encompasses the upper arm, forearm, and wrist, with their scores combined with the REBA worksheet's Table B [11]. Six sets of membership functions were established for the corresponding body parts in REBA, as depicted in Figure 4. In this study, the joint angles were fuzzified using trapezoidal functions, and the REBA intermediate scores were fuzzified using triangular functions. The final REBA score was also obtained using triangular membership functions, while trapezoidal membership functions are used as follows:

$$
\tau(x; a, b, c, d)
\begin{cases}
0, x < a, \\
\dfrac{x-a}{b-a}, a \le x \le b, \\
1, b \le x \le c, \\
\dfrac{x-c}{d-c}, c \le x \le d, \\
0, x > d.
\end{cases}
\tag{3}
$$

The triangular membership function is

$$
\tau(x; a, b, c)
\begin{cases}
\dfrac{x-a}{b-a}, a \le x \le b, \\
\dfrac{c-x}{c-b}, b < x \le c, \\
0, x < a \lor x > c.
\end{cases}
\tag{4}
$$

For joint angles, adjacent membership functions are set to 0.5 to allow for a gradual transition between variables, where a, b, c, and d in formulas (3) and (4) are all real numbers. A fuzzy rule-based system was created, while three sets of 240 rules were developed based on if-then statements. Figure 5 shows the scores for the neck, legs, and trunk based on the rule set A. For example, if the neck score is 2, the leg score is 3, and the trunk score is 3, then the overall score for all three is 5.

Defuzzification is the process of converting fuzzy values into precise and crisp values and can be understood as a mapping from the fuzzy space to the crisp space. Defuzzification is the last step of a fuzzy logic system. In this study, a highly commonly used and reasonable method, the centroid method, was adopted for defuzzification. The centroid method takes the centroid of the area bounded by the membership function curve and the horizontal axis as the final output value. The calculation formula is
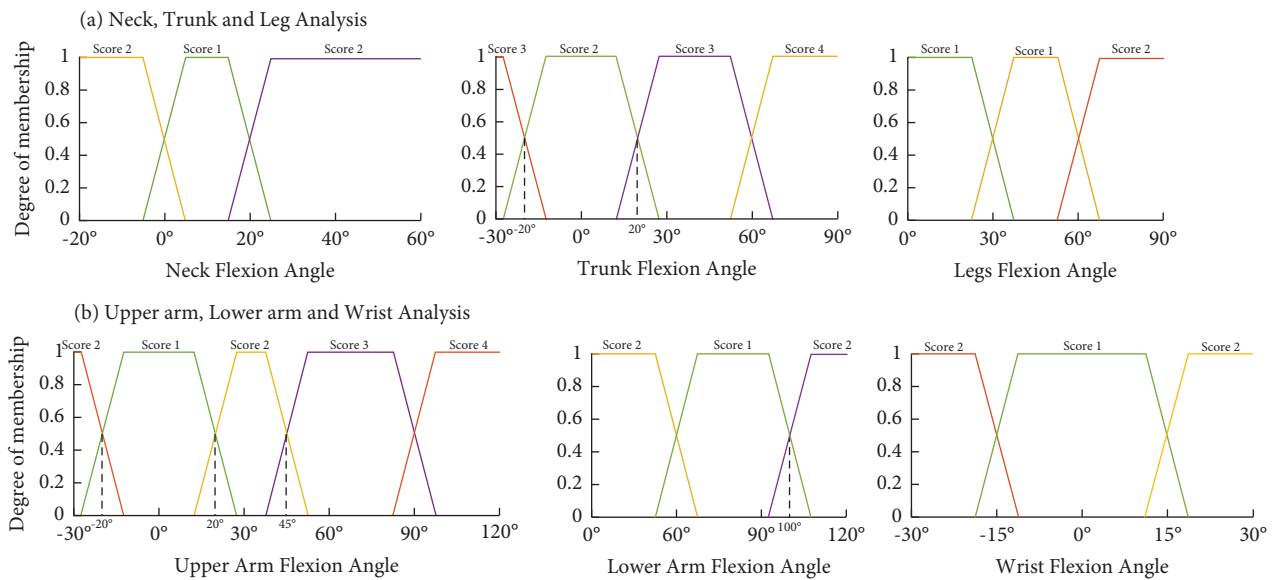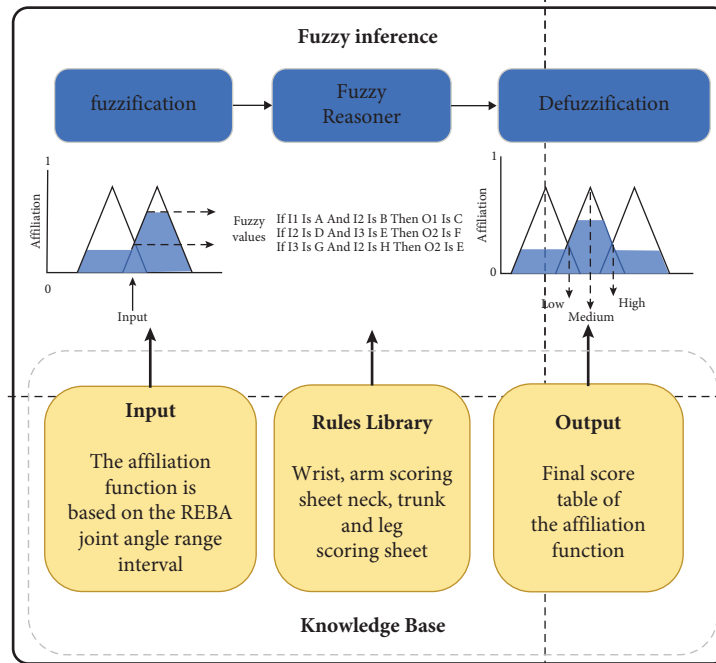
Figure 4: Fuzzy inference algorithm with rules in REBA and six-joint membership function construction.

Figure 5: An illustration of a fundamental if-then rule from REBA's Table A.

$$P = \frac{\int \tau(x)x\,dx}{\int \tau(x)\,dx}. \tag{5}$$

Formula (5) represents the membership value of the output variable, and the maximum membership subset is selected based on the principle of maximum membership value. Fuzzy logic theory can generate stable transition results for joint angle changes. The final evaluation score also gradually transitions, which avoids sudden changes in REBA evaluation scores and improves the method's reliability.

The evaluation is completed using the Fuzzy Logic Toolbox in MATLAB based on the determined input variables, output variables, their membership functions, and fuzzy rules. Finally, scores related to activity types are added. Ultimate REBA scores range from 1 to more than 11, with higher scores indicating a greater risk of WMSDs. Table 2 shows these scores and their corresponding action levels.

3.3. Load Estimation Based on Biomechanical Analysis.

In this study, a novel foot pressure sensor called Moticon was utilized to measure the total weight of workers, which includes both their own weight and external pressure. The insole can be attached to almost any type of footwear and wirelessly transmit data through the ANT service. The insoles are fitted with 26 pressure sensors (13 per insole) to determine the average pressure in the corresponding area. Equation (6) illustrates how one accomplishes this by multiplying each sensor's pressure by its area to determine the insole's overall ground response force.

$$\begin{bmatrix} F_R \\ F_L \end{bmatrix} = \frac{S}{N+1} \sum_{n=0}^{N} \begin{bmatrix} P_{R,n} \\ P_{L,n} \end{bmatrix}, \tag{6}$$

where F_L, F_R are the ground reaction forces of the left and right feet. S is the plantar contact area of each foot ($S = 150\,cm^2$). N is the largest sensor number. n is the number of each sensor; $P_{L,n}, P_{R,n}$ are the pressure values of the left and right feet. The pressure sensor was zeroed before the start of the experiment, and the OpenGo auto-zeroing mode was always active. It is based on an algorithm that continuously checks the sensor zero position and compensates for sensor offsets and drifts. Sensor offsets and drifts that may occur due to shoelace and temperature variations. We use the OpenGo App for sensor calibration. Individual calibration of the pressure sensor zeroing reduces the total force error to less than 5%.

In the current study, human joint torque can be estimated by combining pressure insoles and computer vision [36, 43]. We collected the operator's ground reaction forces F_L and F_R from the pressure insole, combined them, and subtracted our own gravity from them to obtain the external loads. Next, we utilize a pose estimation technique to obtain joint positional information and angles and compute the torques at the end-segment joints (left and right wrist and ankle). Then, we calculate the torque of other non-end-segment joints in turn, and the whole process is shown in Figure 6. Finally, the work load of each joint is estimated according to the maximum load capacity of different joints.

TABLE 2: The REBA method's final risk score and response.

REBA score	Risk level	Response
1	Negligible risk	No change needed
2-3	Low risk	Change may be required
4–7	Moderate risk	Further investigate changes soon
8–10	High risk	Investigation and change implementation
11–15	Very high risk	Implement change

Typically, the external load is located at the hands and feet (ground reaction forces) during handling tasks. Both dual-arm and single-arm working styles are taken into consideration when assessing the force at the hands. The working method is identified by comparing the angles of the left and right shoulder and elbow joints. The working style is categorized as two-handed if the angles of the left and right arms are the same. Otherwise, the working method is determined to be the single-arm working method. The external load on the worker's dominant hand also needs to be considered. The mass of the particle i is assumed as m_i with corresponding weight $G_i = m_i g$. The total weight of the worker is denoted as G_h and its corresponding mass is m_h. There are 16 joint points in the human skeleton diagram shown in Figure 2, thus $G_h = \sum_{i=1}^{16} G_i$ and $m_h = \sum_{i=1}^{16} m_i$. The external load force is assumed as M_e, and its mass is denoted as m_e.

After detecting the workers' postures (the three-dimensional coordinates of the body's joints) in Section 3.1 and measuring the pressure data using pressure insoles, we calculated the torque of each joint using biomechanical analysis and Newton's laws of motion. For biomechanical analysis, the human skeleton can be simplified to a hinged linkage structure, with the bone corresponding to the lever and the joint representing the hinge. This simplification was utilized for calculations. During the analysis, it was presumed that the main joints' movement of the worker's body was steady and unhurried and that the joints were in a state of equilibrium.

The human body's joint torque is mainly generated by the muscles surrounding the joint under the muscle torque arm. The analysis methods vary according to the position of the joint in the body segments and are mainly divided into end-segment joint torque and non-end-segment joint torque. End-segment joints mainly refer to the joints that connect to only one body segment of the human body, while non-end-segment joints mainly refer to joints that connect to multiple body segments of the human body. For a non-terminal body segment i, let the position of the far-end joint of the segment be P_{i-1}, the position of the near-end joint be P_i, the mass of the segment be m_i, and the center of mass be located at G_i. To calculate the joint torque $\overrightarrow{\tau_i}$ at the near-end joint of the segment, it is necessary to determine the joint torque $\overrightarrow{\tau_{i-1}}$ at the far-end joint of the segment. A static equilibrium torque equation can be established at the near-end joint of the segment:

$$\overrightarrow{\tau_i} + \overrightarrow{\tau_{i-1}} + \overrightarrow{P_i G_i} \times \overrightarrow{M_i} = 0,$$
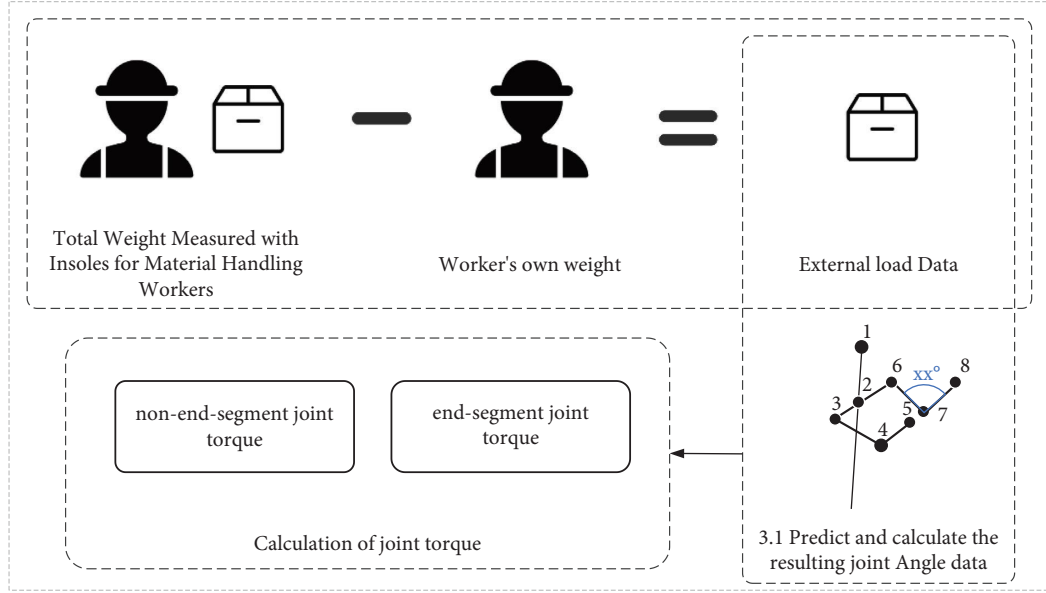$$\overrightarrow{M_i} = m_i \cdot \overrightarrow{g}. \tag{7}$$

FIGURE 6: Calculation of joint torque with smart insoles.

The vector $\overrightarrow{M_i}$ represents the gravitational force acting on the body segment at its center of mass, as shown in Figure 7 for the elbow joint.

For the distal segment i, assuming the proximal joint position is P_i the mass of the segment i is m_i, and the position of its center of mass is G_i. The segment i bears the external force of the external weight m_e, and the position of the center of mass of the external weight is P_e. Therefore, a static equilibrium torque equation can be established at the proximal end of the segment i to calculate the joint torque $\overrightarrow{\tau_i}$, as shown in the following formula:

$$\overrightarrow{\tau_i} + \overrightarrow{P_iP_e} \times \overrightarrow{M_e} + \overrightarrow{P_iG_i} \times \overrightarrow{M_i} = 0,$$
$$\overrightarrow{M_i} = m_i \cdot \overrightarrow{g}, \qquad (8)$$
$$\overrightarrow{M_e} = m_e \cdot \overrightarrow{g}.$$

The vector $\overrightarrow{M_i}$ represents the gravitational force acting on the segment at its center of mass, and $\overrightarrow{M_e}$ represents the gravitational force of any external weight the segment is bearing. Therefore, the static equilibrium equation for joint torque can be derived as follows:

$$\overrightarrow{\tau_i} = -\left(\overrightarrow{T} + m_i \times \overrightarrow{P_iG_i} \times \overrightarrow{g} \right). \qquad (9)$$

The vector $\overrightarrow{T}$ represents the external torque applied to the body segment:

$$\overrightarrow{T} = \begin{cases} \overrightarrow{\tau_{i-1}}, & \text{Segment } i \text{ is a non-terminal segment,} \\ m_e \times \overrightarrow{P_iP_e} \times \overrightarrow{g}, & \text{Segment } i \text{ is a terminal segment.} \end{cases}$$
$$(10)$$

This section aims to evaluate the workload of a worker based on joint torques. It takes into consideration that individuals possess varying load-bearing capacities, and as such, the evaluation of workload should factor in both
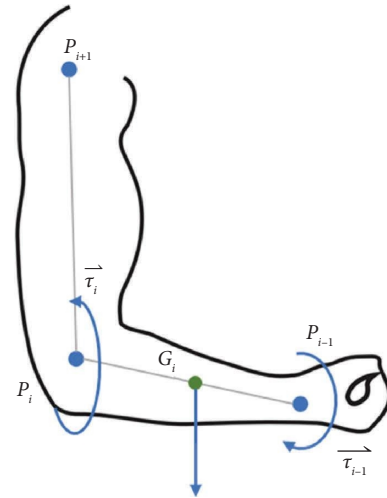

FIGURE 7: Biomechanical analysis of torque in body and non-terminal body segments.

external elements like external loads and postures as well as the worker's load-bearing capacity. To measure human biomechanical capabilities, Maximum Voluntary Isometric Contraction (MVIC) is a widely accepted indicator. The National Isometric Muscle Strength Database Consortium [44] developed a regression equation based on over 500 experiments to predict MVIC using factors such as gender, age, height, and weight. This equation is employed to estimate joint capabilities.

$$\tau_{\max} = \left(a \times \text{gender} + b \times \frac{\text{weight}}{\text{height}^2} - c \times \text{age} + d \right) \times l. \quad (11)$$

The subjects are identified as male = 1 and female = 0; a, b, c, and d are coefficients with values shown in Table 3; $\tau_{\max}$ is the maximum torque that the joint can withstand (N/m); l

TABLE 3: Joint capability regression coefficients.

Joint	a	b	c	d
Left shoulder	14.64	0.29	0.18	19.59
Right shoulder	16.26	0.17	0.17	23.35
Left elbow	10.63	0.05	0.11	19.66
Right elbow	11.24	0.07	0.13	22.78
Left hip	18.75	0.47	0.29	36.05
Right hip	19.19	0.66	0.33	34.44
Left knee	7.67	0.14	0.17	21.10
Right knee	8.78	0.08	0.16	22.47

is the torque arm length (m) when measuring the external load; and since the joint angle in the experiment is a right angle, the torque arm is equal to the length of the corresponding bone. Age, weight, and height are measured in years, kilograms, and meters, respectively.

The joint workload can be calculated on the basis of the existing joint torque τ (N) and the maximal load capacity $\tau_{\max}$ (N):

$$\text{workload} = \frac{\tau}{\tau_{\max}} \times 100\%. \quad (12)$$

4. Experiment

4.1. Instrumentation. A total of 6 male volunteers (age: 23.4 ± 1.0 years, height: 1.78 ± 0.17 m, and weight: 70 ± 2.7 kg) and 4 female volunteers (age: 22.8 ± 1.2 years, height: 1.62 ± 0.05 m, and weight: 51 ± 2.7 kg) were recruited for this study. All volunteers who participated in the experiment did so voluntarily and had satisfactory physical fitness. They did not exhibit any symptoms of musculoskeletal diseases. In addition, they were capable of completing the handling task independently. Before the experiment, all volunteers completed personal information and informed consent forms. A laptop computer with an Intel (R) Core (TM) i5-12490F 3.00 GHz CPU and an NVIDIA GeForce RTX 3060 Ti GPU running Windows 10 was used to run the relevant code and algorithms developed in this study. A smartphone (iPhone 11) was used to collect video data of the handling process. Two pressure sensors (OpenGo and Moticon GmbH) were placed inside the volunteers' shoes to synchronously collect the load data of the people during the handling task, while a tripod was used to keep the smartphone in a fixed position.

4.2. Experimental Setting and Procedure. The experimental setting is shown in Figure 8, and all experiments were conducted at the same time of day to ensure consistent sunlight intensity using a fixed light source. The camera was fixed at a distance of 3 m from the sagittal plane and 1.25 m above the ground. During the experiment, participants were asked to transport a 10 kg box, simulating the process of material handling. The experiment consisted of four parts: (1) participants walked to the box on the right, (2) participants squatted to lift the box, (3) participants walked with the box to the platform on the left, and (4) participants placed the box on the platform. After completing one set of

activities, participants rested for 30 seconds before repeating the experimental task, and then a different participant performed the experiment. Each person completed two sets of experiments, resulting in a total of 20 sets of video frame data and OpenGo sensor data being collected.

4.3. Data Collection. The three-dimensional pose estimation method was employed to accurately extract the three-dimensional joint positions from the video frames. For each frame, the resultant data are a 16×3 matrix containing the accurate three-dimensional coordinates of the 16 joints. The video clips were meticulously divided into 600 frames, each lasting approximately 20 seconds, and underwent thorough three-dimensional pose estimation to obtain the precise joint's 3D coordinates. The extracted angles were subsequently calculated and skillfully utilized for accurate fuzzy Rapid Entire Body Assessment (REBA) analysis.

The pressure data collected were utilized for evaluating the weight of the worker and other loads on them. Intelligent shoe insoles were used to assess total weight or ground response force. The pressure data from each sensor was recorded to determine the average pressure in the corresponding area. Figure 8 shows the visual distribution of the pressure values of the left and right shoe insoles during the process of carrying and lifting the cardboard box by the subjects. The pressure measurements from each of the 13 pressure sensors on the right shoe insole are displayed in Table 4. 30 frames per second (fps) of video data were captured, while the shoe insole pressure data were recorded at a frequency of 50 frames per second.

4.4. Results. The experimental process of the volunteers carrying boxes is shown in Figure 9, which includes the recording of 8 keyframes of motion, corresponding to 2D joint estimation skeletal images and estimate of 3D joint coordinate images. Our shooting angle allows the sagittal plane of the volunteers to be clearly photographed while also observing the right half of the volunteer's body. The recognition results show that even when there is occlusion of the right half of the volunteer's body relative to the left half and when there is some occlusion of the left arm during the process of carrying the box, there is no recognition error in the 2D joint recognition. Therefore, the obtained 3D joint coordinates match the coordinates of the volunteer's actual activity.

The 3D pose estimation method in this paper was compared to the IMU sensor measurement method for recognition accuracy. The experiment was the same as before, containing subjects completing four operational tasks. In the experiments, subjects wore inertial motion capture devices while video recording was performed to capture joint positions, and a total of 600 video frames were captured. We were able to acquire data from 16 body joints from pose recognition, while wearing the IMU sensor only captured the position information of 14 joints (ignoring the neck and buttocks joints information). The experiment procedure is shown in Figure 10.
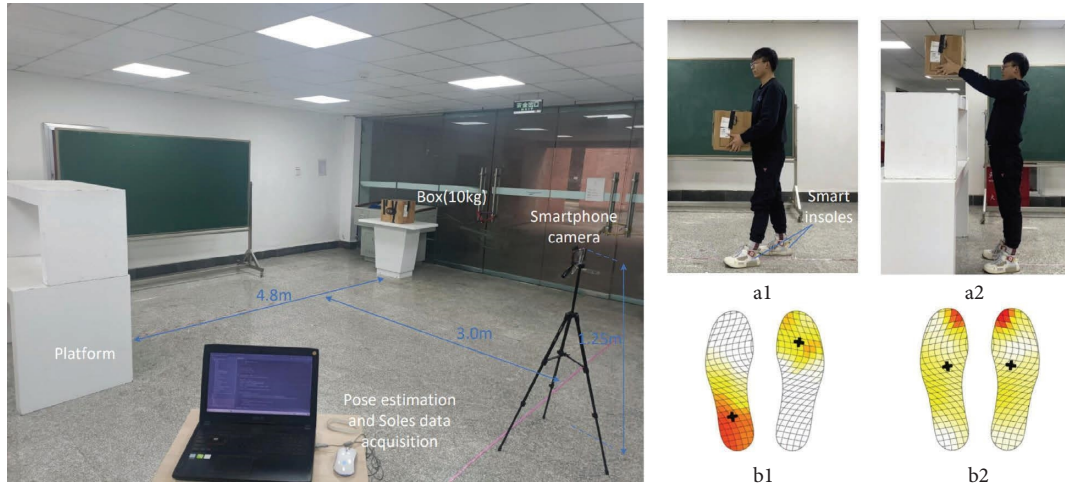
FIGURE 8: Experimental scene configuration and pressure distribution of two different actions on shoe insoles.

TABLE 4: Values for each of the 13 pressure sensors on the right insole.

Sensor number	Pressure (N/cm²)
0	1.25
1	1.50
2	1.00
3	0.50
4	1.00
5	3.00
6	0.25
7	5.25
8	2.50
9	5.75
10	5.5
11	4.24
12	5.25

First, we compared the joint point positions estimated from the 3D pose in this paper with the joint positions measured by the IMU sensor, as shown in Figure 11(a). The errors of most frames fall within the range of 2.25 cm to 4.75 cm, with an average error of 4.78 cm and a standard error of 1.47 cm. Next, we compared the joint angle values computed based on the method in this paper and the data from the IMU sensor, as shown in Figure 11(b). More than 470 video frames had errors in the range of −5° to 5°, with an average angular error of −0.66° and a standard error of 9.25. Only a very small number of video frames had errors in the range of −20° to 20°, which was attributed to the fact that the limbs overlapped and occluded heavily at certain moments, resulting in large joint angle errors, usually in the right and left knee joints. Overall, the method in this paper has higher accuracy compared to IMU measurements. In addition, the method in this paper does not need to build an experimental environment for IMU sensors and does not interfere with the operator's normal work, which makes it more portable.

5. Discussion

5.1. Comparison and Discussion of Experiments between REBA and Improved REBA. Figures 12 and 13 show the REBA scores and risk levels of the subjects during a 20-second (600 frames) moving process. The data were calculated by averaging the risk assessment results of 10 volunteers. We compared two evaluation methods: the traditional REBA scoring method and the improved REBA evaluation method based on fuzzy logic, which we refer to as FREBA in the figures. In the REBA score chart, the traditional evaluation method uses a total score, resulting in a stepwise ladder line in the chart. As joint angles change with time during the lifting process, when one or more joints reach the scoring threshold, the REBA score fluctuates. The FREBA score obtained after fuzzy processing is a decimal, hence the smooth curve in the chart, which is more accurate than traditional REBA evaluation and avoids the problem of fluctuating scores. In Figure 13, the risk level ladder line of the traditional REBA evaluation fluctuates due to the influence of the score, while the FREBA evaluation result is stable without fluctuations and better matches the posture and risk status of the subjects at the time.

Table 5 presents the joint angles, REBA scores, FREBA scores, and risk levels of participants in four missions. In mission 1, participants performed normal walking without any risk. In mission 2, participants squatted down to lift a cardboard box, resulting in high scores due to the high hip joint and thigh bending angles. Therefore, it is necessary to adjust the current action as soon as possible and minimize the carrying work at a very low point in the future mission. In mission 3, participants carried the cardboard box while walking, resulting in a relatively low score, but the lower arm was kept at around 90° and needed appropriate adjustments. Meanwhile, the gravity of the load and the upper arm load will be analyzed in the following text. In mission 4,
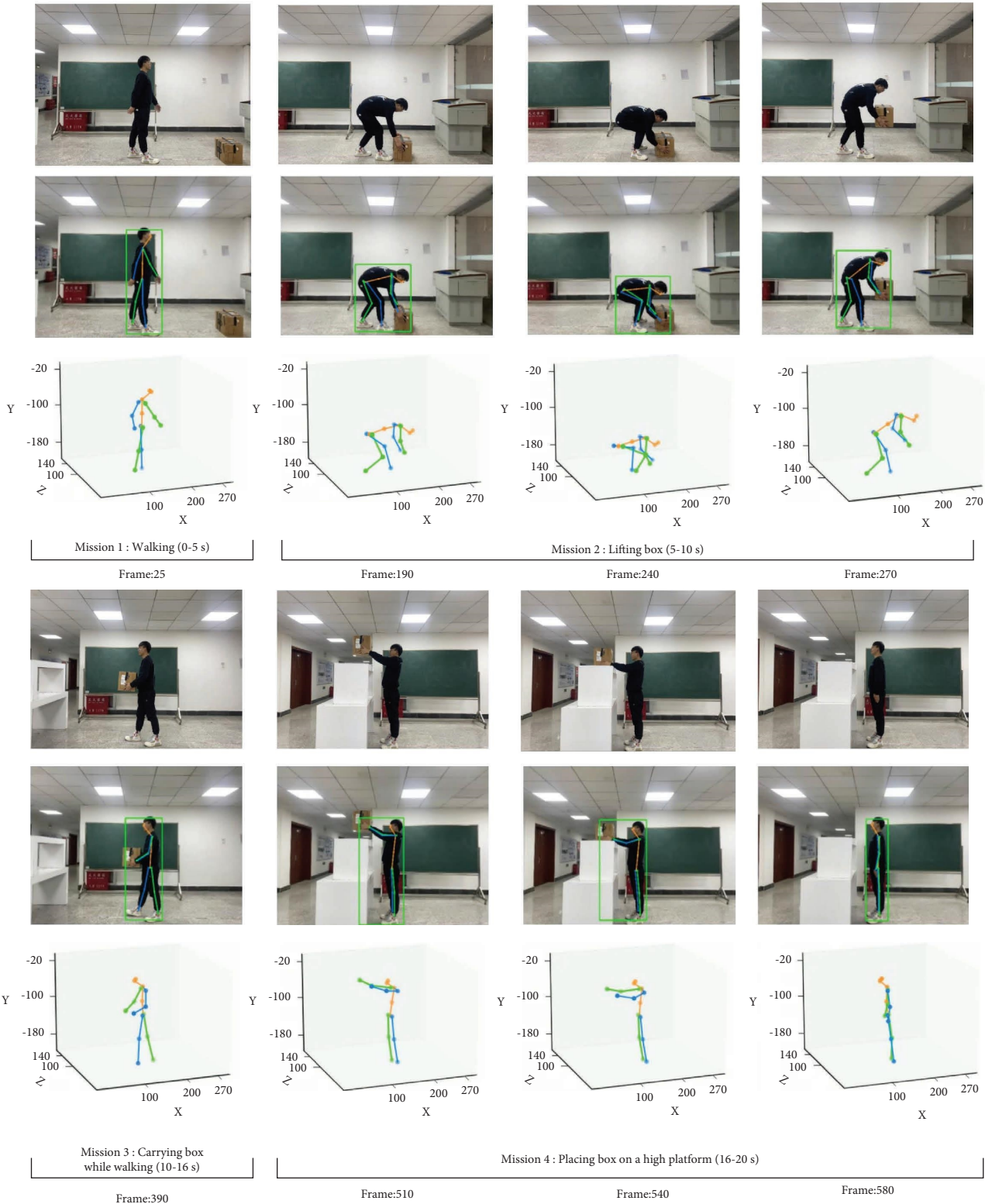
FIGURE 9: The experimental process of volunteer moving box includes (original video frames, 2D pose estimation results, and 3D pose estimation results).

participants lifted the cardboard box onto a higher platform, resulting in a shoulder joint angle of 107.4°, an elbow joint angle of 22.8°, and a risk level of 3, indicating the need to complete the mission as soon as possible. The table also

compared the results of traditional REBA and FREBA scores, with a Spearman correlation coefficient [45] of 0.817. The Spearman rank correlation coefficient critical value table showed that with a sample size of 6, if the correlation
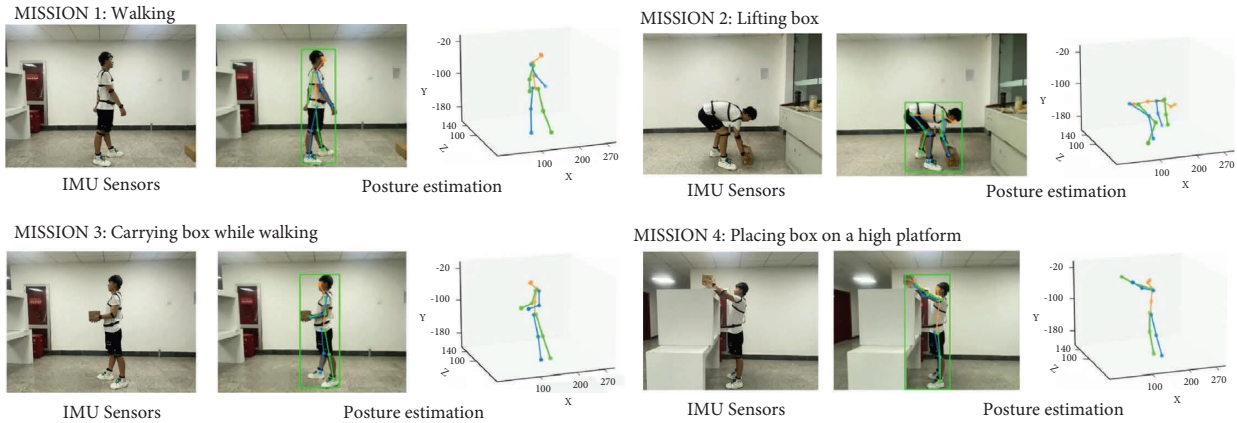
FIGURE 10: Comparison experiment of the recognition accuracy of our method with IMU sensors.
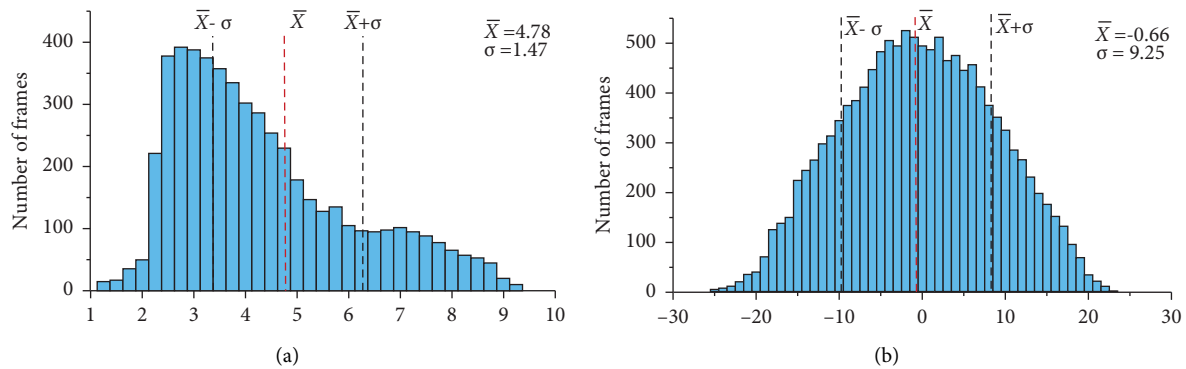

(a)

(b)

FIGURE 11: Distribution of joint positions and joint angle estimation error. (a) The error of joint positions (cm). (b) The error of angles (°).
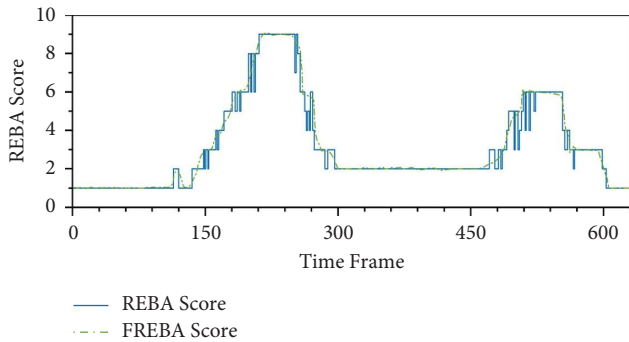

FIGURE 12: The REBA scores corresponding to the two evaluation methods during the handling process.
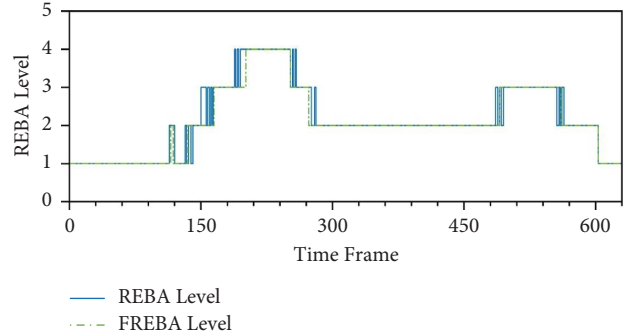
FIGURE 13: The REBA level corresponding to the two evaluation methods during the handling process.

coefficient r is greater than 0.727, there is 99% confidence that two random variables are related. Therefore, at a confidence level of $p = 0.01$, the method can effectively improve the REBA evaluation method and has high reliability.

5.2. Discussion of Experimental Results for Joint Torque and Joint Load Assessment.

We obtained the torque data of 10 volunteers moving boxes through the use of pressure insoles and biomechanical calculations and averaged them. The torque data in the figure did not take into account the

directional factors and can be regarded as absolute values. Figure 14 includes eight joint torque curves and indicates the periods and torque values of four keyframes for different missions. In mission one, the elbow and shoulder joint torques of the volunteers did not change significantly, but the hip and knee joint torques showed periodic fluctuations due to leg movements during walking. When volunteers performed mission two, squatting to lift boxes, the torques of various joints significantly increased. The knee joint torque increased to 80 N/m, and the hip joint torque increased to 70 N/m, corresponding to the REBA score and risk

TABLE 5: Joint angles, REBA scores, and risk levels in missions 1–4.

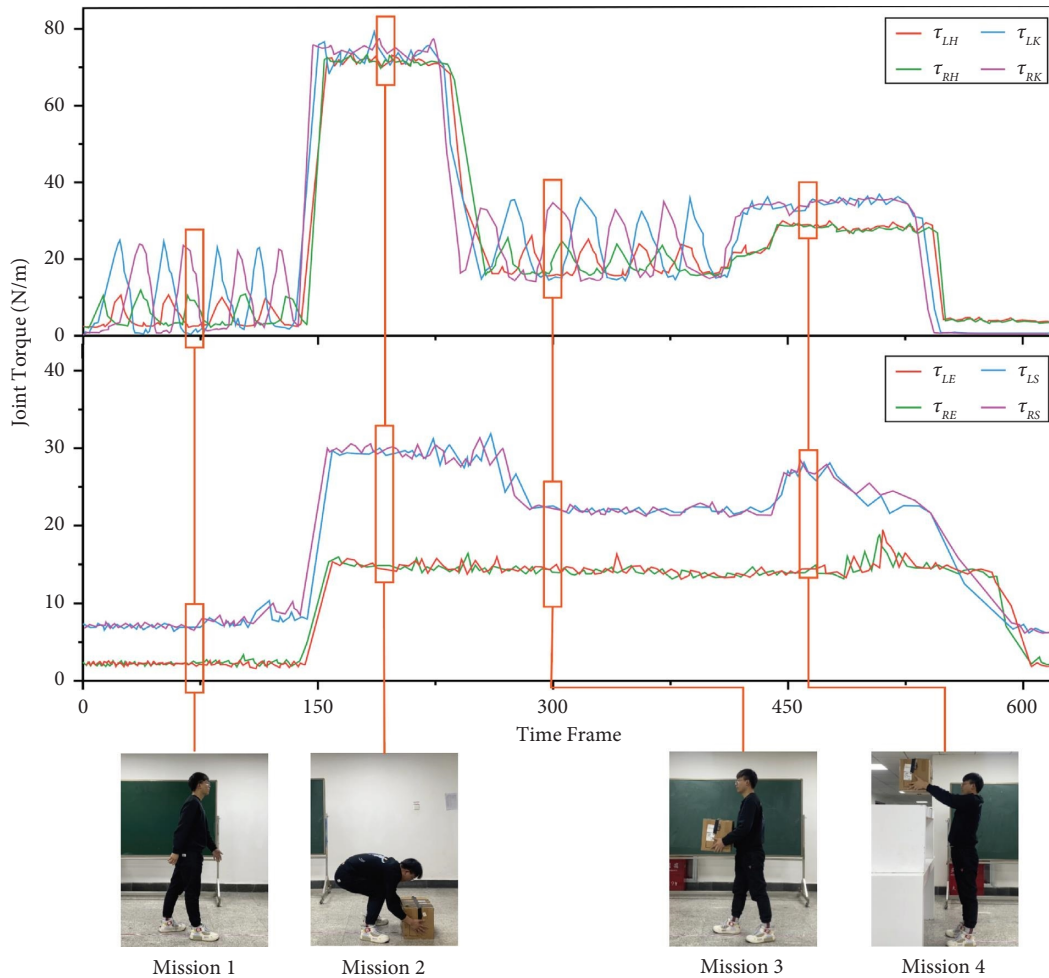| Mission	Neck	Trunk	Leg	Upper arm	Lower arm	Wrist	REBA score	FREBA score	Risk level
1	3.6°	0°	5.1°	15.6°	25.2°	4.5°	1	1.04	1
2	25.2°	56.6°	72.8°	57.5°	34.5°	0°	9	8.48	4
3	3.2°	1.4°	6.4°	39.7°	92.8°	1.2°	2	2.56	2
4	2.6°	−1.3°	0°	107.4°	22.8°	1.7°	6	6.54	3

FIGURE 14: The joint torque of the participants during the handling process.

assessment level we evaluated. In mission three, when volunteers carried boxes while walking, the knee and hip joint torques maintained the wave-like pattern of walking torques, but the torques of each joint were relatively higher than those in mission one, which was caused by the external workload of lifting the box. In mission four, due to the need to lift the box to a higher platform for placement, the torque values of the left and right shoulders of the volunteers also increased to a high point of 28.16 N/m, after which the entire lifting process was completed. Through the changes in the torque curves, the torque situation of each joint of the volunteers during the entire lifting process can be intuitively observed, and these data can be further studied as the working load of each joint.

According to the physiological information of volunteers and formula (11), we calculated the joint capacity of volunteers and the joint workload ratios corresponding to the four missions. By combining Table 6 and Figure 15, we found that the joint workload ratios of the subjects were highest in mission 2, with workload ratios of the left and right shoulder and hip joints approaching 30%, which is consistent with the previous risk assessment. Due to the addition of the external workload of the cardboard box in missions 1 and 3, the hip joint workload ratio and knee joint workload ratio increased by about 4%. In mission 4, because it required the person to lift the arm, the workload ratio of the left and right shoulder joints rose to 27.77% and 26.75%, respectively, and other joint workload ratios increased

TABLE 6: Examples of mission 1–4 findings from the combined workload assessment.

| Joint torque	Joint capacity (N/m)	Joint workload (%)			
		Mission 1 (%)	Mission 2 (%)	Mission 3 (%)	Mission 4 (%)
Left shoulder	100.34	15.70	29.10	19.86	27.77
Right shoulder	103.47	16.24	28.89	20.30	26.75
Left elbow	125.45	5.06	14.02	15.85	14.54
Right elbow	110.46	5.28	15.93	16.42	14.96
Left hip	256.78	7.59	29.79	10.95	9.73
Right hip	264.25	8.51	28.94	10.21	10.11
Left knee	307.45	9.21	26.02	13.07	13.19
Right knee	297.64	9.58	26.87	12.64	13.78
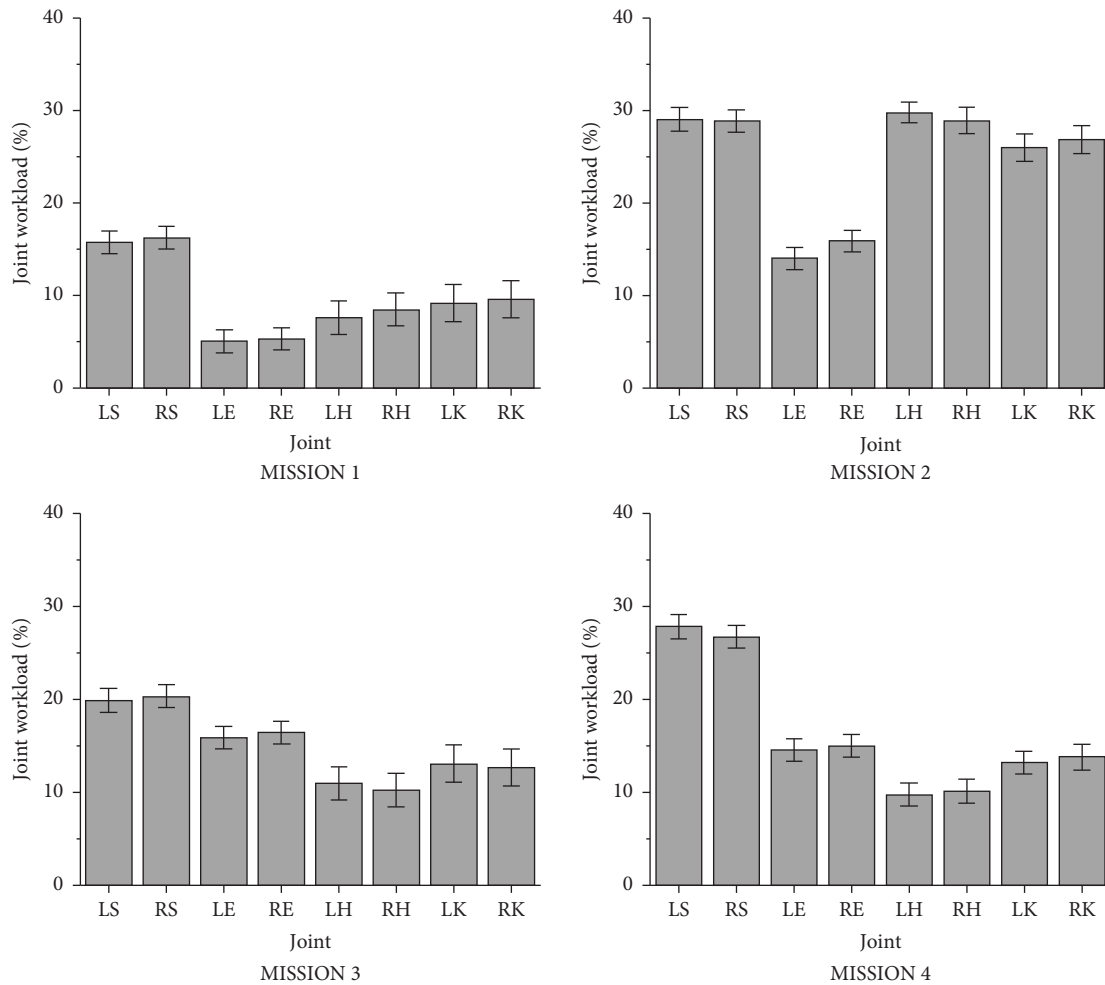
FIGURE 15: Joint workloads of the participants in missions 1–4.

slightly compared to mission 1. The joint workload ratio during the entire handling process did not exceed 40%, which was because the selected cardboard box was relatively light and the volunteers' motion range was relatively standardized.

5.3. Superiority Compared to Existing Research.

Our research has the following advantages: first, we propose a computer vision-based postural risk assessment method, and by comparing the recognition accuracy with wearable IMU sensors, the results illustrate that the method has higher recognition accuracy and better portability. Second, in this paper, we improved the traditional REBA risk assessment method by introducing the fuzzy logic theory, which avoids the sudden change of the overall risk level caused by the input of a specific angle and is more capable of expressing the score transition during the movement of body joints. FREBA is more suitable for the postural risk assessment based on vision technology in the current study. Third, we

also included the assessment of joint workload to make the postural risk assessment more complete. The risk assessment based on vision technology in the current study has some limitations. For example, if an operator moves two objects with large mass differences in sequence with an identical posture, the scores of the risk assessment by machine vision are the same, but the fatigue level of the human being is completely different. Therefore, in this study, the above problem can be solved by estimating the workload of different joints through noninvasive pressure sensors. This method is the same as the machine vision method and will not affect the normal operation of the workers. It can be widely used in the construction industry, logistics handling operations, and other practical work scenarios to assess the postural risk of the workers. It can be used to take timely preventive measures to improve the occupational health and work efficiency of the workers.

5.4. Limitations and Future Work. The methodology proposed in this study aims to monitor, assess, and predict the risk level of WMSDs derived from operational videos and pressure-insole data. There are many ways to apply the method in a company, such as postural risk monitoring and assessment of operators at the actual workplace, operational safety training for new operators, and improvement of a certain work process based on the risk assessment results to reduce the potential risk of WMSDs. In practice, however, there may be problems of occlusion by machines or other objects, so it is important to have a good angle of acquisition of the video, and to place the camera as far as possible in the sagittal plane of the operator, so that the posture of the operator is as fully exposed as possible to the field of view of the acquisition. The estimation of joint workload by means of pressure insoles is done by picking up the reaction force of the ground to obtain the external load, so the operator's feet cannot leave the ground. Leaning or sitting on the ground can cause estimation errors and should be avoided.

The experimental results show that the proposed method in this paper is an accurate, reliable, time-saving, and convenient MSD risk assessment method. This method can not only accurately estimate posture risk but also estimate joint torque and workloads, making it a useful tool for determining risk assessment in actual work environments. However, this study also has certain limitations. More volunteers are needed to represent different labor forces, such as different body types, body mass index categories, and genders. In biomechanical load estimation, we have always assumed that human motion is a uniform process. However, if the worker's motion is unstable, acceleration can increase joint torque, and the external load estimation method used in this study involves subtracting the pressure detected by the insole from the worker's own weight, which means that all the pressure on the worker in the work is on the feet and does not apply to situations where the worker is sitting or sharing the weight on the knee. The methodology proposed in this study aims to monitor, assess, and predict the

risk level of WMSDs derived from operational videos and pressure-insole data. There are many ways to apply the method in a company, such as postural risk monitoring and assessment of operators at the actual workplace, operational safety training for new operators, and improvement of a certain work process based on the risk assessment results to reduce the potential risk of WMSDs. In practice, however, there may be problems of occlusion by machines or other objects, so it is important to have a good angle of acquisition of the video, and to place the camera as far as possible in the sagittal plane of the operator, so that the posture of the operator is as fully exposed as possible to the field of view of the acquisition. The estimation of joint workload by means of pressure insoles is done by picking up the reaction force of the ground to obtain the external load, so the operator's feet cannot leave the ground. Leaning or sitting on the ground can cause estimation errors and should be avoided.

To address the limitations mentioned above, future research will include: (1) incorporating acceleration data if available to analyze joint torque through kinematics; (2) developing more precise methods for estimating external load, such as utilizing deep learning algorithms to identify carried objects and using this information to assist in weight estimation; and (3) exploring whether a new quantitative standard can combine posture risk and joint load for human ergonomics evaluation and using more actual work scenarios to train 3D motion estimation algorithms, especially in scenarios where there are high visual obstacles between workers and cameras.

6. Conclusions

This study proposes a noninvasive method for assessing the risk of working posture and analyzing workload by using computer vision algorithms and smart shoe insoles to collect posture data of workers during lifting operations and finally outputs the worker's REBA assessment data and joint workload data. First, a 3D pose recognition method based on MMpose is proposed and verified to obtain human 3D skeletal data and calculate human joint angles. Fuzzy logic is introduced into the REBA risk assessment to avoid the problem of sudden jumps or drops in the assessment results caused by small changes in joint angle inputs, and the experiment shows that the REBA evaluation method with fuzzy logic fusion is more accurate and reliable. The torque information of each joint is obtained by using inverse kinematics to calculate the human 3D skeletal data and pressure shoe insole data, and the workload ratio of different joints is calculated. This study provides a new approach for practical work posture risk assessment and workload analysis, which can help improve ergonomics based on machine vision.

Data Availability

The data presented in this study are available on request from the corresponding author. The data are not publicly available to protect the subjects' privacy.

Conflicts of Interest

Acknowledgments

References

[1] P. K. Hanumegowda and S. Gnanasekaran, "Prediction of work-related risk factors among bus drivers using machine learning," *International Journal of Environmental Research and Public Health*, vol. 19, no. 22, Article ID 15179, 2022.

[2] P. Paudel, Y. Kwon, D. Kim, and K. Choi, "Industrial ergonomics risk analysis based on 3d-human pose estimation," *Electronics*, vol. 11, no. 20, p. 3403, 2022.

[3] F. Yang, N. Di, W. Guo et al., "The prevalence and risk factors of work related musculoskeletal disorders among electronics manufacturing workers: a cross-sectional analytical study in China," *BMC Public Health*, vol. 23, no. 1, p. 10, 2023.

[4] F. Rybnikár, I. Kačerová, P. Hořejší, and M. Šimon, "Ergonomics evaluation using motion capture technology—literature review," *Applied Sciences*, vol. 13, no. 1, p. 162, 2022.

[5] A. Reiman, J. Kaivo-Oja, E. Parviainen, E. Takala, and T. Lauraeus, "Human factors and ergonomics in manufacturing in the industry 4.0 context–a scoping review," *Technology in Society*, vol. 65, Article ID 101572, 2021.

[6] I. Van Crombrugge, S. Sels, B. Ribbens, G. Steenackers, R. Penne, and S. Vanlanduit, "Accuracy assessment of joint angles estimated from 2d and 3d camera measurements," *Sensors*, vol. 22, no. 5, p. 1729, 2022.

[7] P. B. Rodrigues, Y. Xiao, Y. E. Fukumura et al., "Ergonomic assessment of office worker postures using 3d automated joint angle assessment," *Advanced Engineering Informatics*, vol. 52, Article ID 101596, 2022.

[8] H. Yuan and Y. Zhou, "Ergonomic assessment based on monocular rgb camera in elderly care by a new multi-person 3d pose estimation technique (romp)," *International Journal of Industrial Ergonomics*, vol. 95, Article ID 103440, 2023.

[9] O. Karhu, P. Kansi, and I. Kuorinka, "Correcting working postures in industry: a practical method for analysis," *Applied Ergonomics*, vol. 8, no. 4, pp. 199–201, 1977.

[10] T. R. Waters, V. Putz-Anderson, A. Garg, and L. J. Fine, "Revised niosh equation for the design and evaluation of manual lifting tasks," *Ergonomics*, vol. 36, no. 7, pp. 749–776, 1993.

[11] S. Hignett and L. Mcatamney, "Rapid entire body assessment (reba)," *Applied Ergonomics*, vol. 31, no. 2, pp. 201–205, 2000.

[12] L. Mcatamney and E. Nigel Corlett, "Rula: a survey method for the investigation of work-related upper limb disorders," *Applied Ergonomics*, vol. 24, no. 2, pp. 91–99, 1993.

[13] M. L. Nunes, D. Folgado, C. Fujao et al., "Posture risk assessment in an automotive assembly line using inertial sensors," *IEEE Access*, vol. 10, pp. 83221–83235, 2022.

[14] X. Yan, H. Li, A. R. Li, and H. Zhang, "Wearable imu-based real-time motion warning system for construction workers' musculoskeletal disorders prevention," *Automation in Construction*, vol. 74, pp. 2–11, 2017.

[15] V. M. Manghisi, A. E. Uva, M. Fiorentino, V. Bevilacqua, G. F. Trotta, and G. Monno, "Real time rula assessment using kinect v2 sensor," *Applied Ergonomics*, vol. 65, pp. 481–491, 2017.

[16] A. Abobakr, D. Nahavandi, M. Hossny et al., "Rgb-d ergonomic assessment system of adopted working postures," *Applied Ergonomics*, vol. 80, pp. 75–88, 2019.

[17] Y. Lee and C. Lee, "See: a proactive strategy-centric and deep learning-based ergonomic risk assessment system for risky posture recognition," *Advanced Engineering Informatics*, vol. 53, Article ID 101717, 2022.

[18] L. Li, T. Martin, and X. Xu, "A novel vision-based real-time method for evaluating postural risk factors associated with musculoskeletal disorders," *Applied Ergonomics*, vol. 87, Article ID 103138, 2020.

[19] W. Fang, M. Fu, and L. Zheng, "Continuous ergonomic risk perception for manual assembly operations using wearable multi-sensor posture estimation," *Assembly Automation*, vol. 42, no. 2, pp. 209–217, 2021.

[20] M. N. H. Yunus, M. H. Jaafar, A. S. A. Mohamed, N. Z. Azraai, and M. S. Hossain, "Implementation of kinetic and kinematic variables in ergonomic risk assessment using motion capture simulation: a review," *International Journal of Environmental Research and Public Health*, vol. 18, no. 16, p. 8342, 2021.

[21] Y. Kwon, D. Kim, B. Son, K. Choi, S. Kwak, and T. Kim, "A work-related musculoskeletal disorders (wmsds) risk-assessment system using a single-view pose estimation model," *International Journal of Environmental Research and Public Health*, vol. 19, no. 16, p. 9803, 2022.

[22] A. Altieri, S. Ceccacci, A. Talipu, and M. Mengoni, "A low cost motion analysis system based on rgb cameras to support ergonomic risk assessment in real workplaces," in *International Design Engineering Technical Conferences and Computers and Information in Engineering Conference*, vol. 83983, November 2020.

[23] J. Zhao and E. Obonyo, "Applying incremental deep neural networks-based posture recognition model for ergonomics risk assessment in construction," *Advanced Engineering Informatics*, vol. 50, Article ID 101374, 2021.

[24] J. Wang, D. Chen, M. Zhu, and Y. Sun, "Risk assessment for musculoskeletal disorders based on the characteristics of work posture," *Automation in Construction*, vol. 131, Article ID 103921, 2021.

[25] J. Winkel and S. E. Mathiassen, "Assessment of physical work load in epidemiologic studies: concepts, issues and operational considerations," *Ergonomics*, vol. 37, no. 6, pp. 979–988, 1994.

[26] W. Umer, H. Li, G. P. Y. Szeto, and A. Y. Wong, "Low-cost ergonomic intervention for mitigating physical and subjective discomfort during manual rebar tying," *Journal of Construction Engineering and Management*, vol. 143, no. 10, Article ID 4017075, 2017.

[27] N. A. Bowling and C. Kirkendall, "Workload: a review of causes, consequences, and potential interventions," *Contemporary Occupational Health Psychology: Global Perspectives on Research and Practice*, vol. 2, no. 2, pp. 221–238, 2012.

[28] D. Roman-Liu, "Comparison of concepts in easy-to-use methods for msd risk assessment," *Applied Ergonomics*, vol. 45, no. 3, pp. 420–427, 2014.

[29] W. P. Neumann, R. P. Wells, R. W. Norman et al., "A posture and load sampling approach to determining low-back pain risk in occupational settings," *International Journal of Industrial Ergonomics*, vol. 27, no. 2, pp. 65–77, 2001.

[30] E. Valero, A. Sivanathan, F. Bosché, and M. Abdel-Wahab, "Musculoskeletal disorders in construction: a review and a novel system for activity tracking with body area network," *Applied Ergonomics*, vol. 54, pp. 120–130, 2016.

[31] W. Kim, J. Lee, N. Tsagarakis, and A. Ajoudani, "A real-time and reduced-complexity approach to the detection and monitoring of static joint overloading in humans," in *2017 International Conference on Rehabilitation Robotics (ICORR)*, pp. 828–834, London, UK, July 2017.

[32] C. A. Gallo, W. K. Thompson, B. E. Lewandowski et al., "Computational modeling using opensim to simulate a squat exercise motion," *NASA Human Research Program Investigators Workshop: Integrated Pathways to Mars*, NASA, Washington, DC, USA, 2015.

[33] S. L. Delp, F. C. Anderson, A. S. Arnold et al., "Opensim: open-source software to create and analyze dynamic simulations of movement," *IEEE Transactions on Biomedical Engineering*, vol. 54, no. 11, pp. 1940–1950, 2007.

[34] M. Senteler, B. Weisse, D. A. Rothenfluh, and J. G. Snedeker, "Intervertebral reaction force prediction using an enhanced assembly of opensim models," *Computer Methods in Biomechanics and Biomedical Engineering*, vol. 19, no. 5, pp. 538–548, 2016.

[35] X. Yang, Y. Yu, H. Li, X. Luo, and F. Wang, "Motion-based analysis for construction workers using biomechanical methods," *Frontiers of Engineering Management*, vol. 4, no. 1, pp. 84–91, 2017.

[36] L. Kong, H. Li, Y. Yu, H. Luo, M. Skitmore, and M. F. Antwi-Afari, "Quantifying the physical intensity of construction workers, a mechanical energy approach," *Advanced Engineering Informatics*, vol. 38, pp. 404–419, 2018.

[37] M. F. A. Afari, Y. Yu, H. Li, A. Darko, J. O. Seo, and A. Wong, "Automated detection and classification of construction workers' awkward working postures using wearable insole pressure sensors," in *1st Postgraduate in Applied Research Conference in Africa*, Accra, Ghana, February 2018.

[38] A. H. Schwartz, T. J. Albin, and S. G. Gerberich, "Intra-rater and inter-rater reliability of the rapid entire body assessment (reba) tool," *International Journal of Industrial Ergonomics*, vol. 71, pp. 111–116, 2019.

[39] S. Dockrell, E. O'Grady, K. Bennett et al., "An investigation of the reliability of rapid upper limb assessment (rula) as a method of assessment of children's computing posture," *Applied Ergonomics*, vol. 43, no. 3, pp. 632–636, 2012.

[40] R. Girshick, "Fast r-cnn," in *Proceedings of the IEEE International Conference on Computer Vision (ICCV)*, pp. 1440–1448, Santiago, Chile, December 2015.

[41] K. Sun, B. Xiao, D. Liu, and J. Wang, "Deep high-resolution representation learning for human pose estimation," in *Proceedings of the IEEE/CVF conference on computer vision and pattern recognition*, pp. 5693–5703, Long Beach, CA, USA, June 2019.

[42] J. Charles, T. Pfister, D. Magee, D. Hogg, and A. Zisserman, "Personalizing human video pose estimation," in *Proceedings of the IEEE conference on computer vision and pattern recognition*, pp. 3063–3072, Las Vegas, NV, USA, June 2016.

[43] Y. Yu, H. Li, W. Umer et al., "Automatic biomechanical workload estimation for construction workers by computer vision and smart insoles," *Journal of Computing in Civil Engineering*, vol. 33, no. 3, Article ID 4019010, 2019.

[44] The National Isometric Muscle Strength NIMS Database Consortium, "Muscular weakness assessment: use of normal isometric strength data," *Archives of Physical Medicine and Rehabilitation*, vol. 77, no. 12, pp. 1251–1255, 1996.

[45] Y. Dodge, "Spearman rank correlation coefficient," *The Concise Encyclopedia Of Statistics*, Springer New York, New York, NY, USA, pp. 502–505, 2008.